ACS Energy LETTERS

http://pubs.acs.org/journal/aelccp

Ultra-Wideband Transparent Conductive Electrode for Electrochromic Synergistic Solar and Radiative Heat Management

Yunfei Rao,[†] Jingyuan Dai,[†] Chenxi Sui,[†] Yi-Ting Lai,[†] Zhe Li, Haoming Fang, Xiuqiang Li, Wei Li, and Po-Chun Hsu*

Cite This: *ACS Energy Lett.* 2021, 6, 3906−3915

Read Online

ACCESS | Metrics & More | Article Recommendations | Supporting Information

ABSTRACT: Electrochromic devices are a key technology to modulate optical and thermal energy for zero-energy buildings. With the sun as the heat source and deep space as the cold source, it would be beneficial to accomplish wideband regulation and control both solar and radiative heat simultaneously to obtain large heating and cooling performance. Here, a flexible ultra-wideband transparent conducting electrode (UWB-TCE) with low sheet resistance (R_s = 22.4 ohm/sq) and high optical transmittance (T_{UV-vis} = 85.63%, $T_{near-IR}$ = 87.85%, and T_{mid-IR} = 84.87%) has been demonstrated to realize an electrochromic device that is capable of synergistic solar and radiative heat management. Enabled by the UWB-TCE, the metal-based electrochromic device can vary its emissivity between 0.12 and 0.94. The device can also switch between solar heating mode (high solar absorptivity and low thermal emissivity) and radiative cooling mode (low solar absorptivity and high thermal emissivity) by controlling the optimal electrodeposition morphology for surface plasmon resonance. The optimal solar absorptivity (α) and thermal emissivity (ε) of solar heating and radiative cooling mode are (α, ε) = (0.60, 0.20) and (0.33, 0.94), respectively. The UWB-TCE and dual-band solar and mid-IR electrochromic device can bring vast opportunities for applications in heat management, camouflage, display, and building energy efficiency.

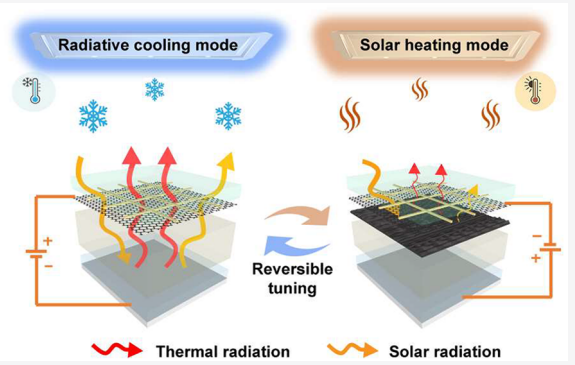

As global warming and climate change worsen, developing effective heat management using renewable energy instead of fossil fuels has become a pivotal subject. Residential use accounts for more than 37% of electricity consumption in the United States. For building indoor temperature control, which alone accounts for more than 15% of national energy consumption,[1−3] solar heating and radiative cooling are two of the most effective sustainable approaches. Solar heating is already a commercially successful technology, thanks to decades of efforts in both theory development and experimental demonstration.[4−11] In recent years, subambient daytime radiative cooling was demonstrated by photonic engineering of the materials that create high solar reflectivity and high emissivity in the mid-infrared atmospheric window.[12−15] These seminal works have led to a series of contributions reporting improved applicability, cost-effectiveness, and system-level innovation.[16−28]

While both solar heating and radiative cooling can save energy, their single functionality can be a potential barrier for wide employment. Because of the seasonality of most regions of the U.S. and major cities in the world, the optimal modes of thermal management are different throughout the years, if not months or days. An ideal building envelope for the future net-zero-energy buildings[3,29,30] should be capable of adapting its optical and thermal property in response to different parameters such as ambient conditions, occupants' demands, and electricity supply.

To create a smart building envelope that can switch between solar heating and radiative cooling, the device must be tunable in a substantially wide bandwidth: from ultraviolet (~300 nm in wavelength) to mid-infrared (mid-IR, ~25 μm for ambient thermal radiation or ~14 μm for atmospheric window). Ideally, low solar absorptivity and high thermal emissivity works in radiative cooling state, and high solar absorptivity and

Received: July 16, 2021
Accepted: October 11, 2021
Published: October 14, 2021

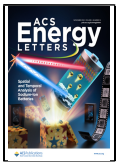

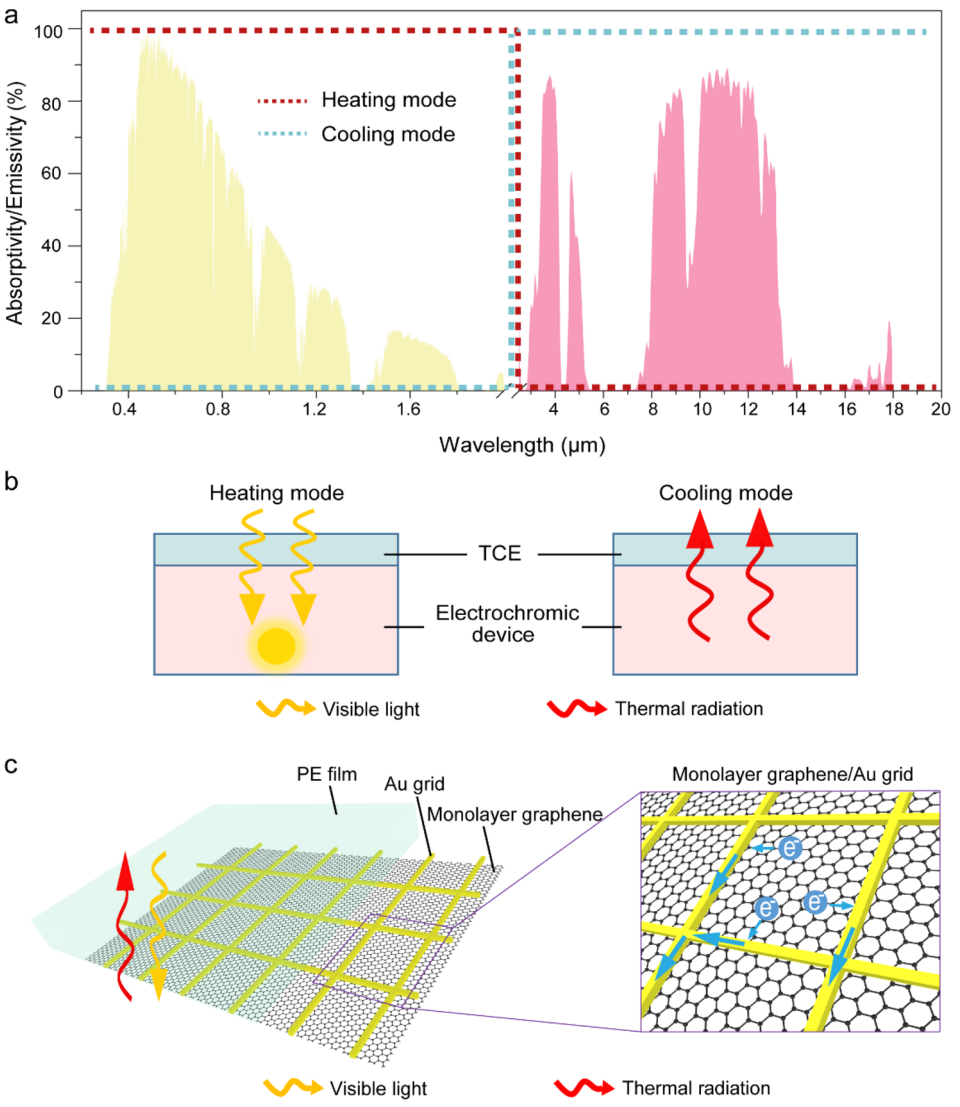

Figure 1. Ultra-wideband transparent conducting electrode (UWB-TCE) for electrochromic synergistic solar and radiative heat management. (a) Ideal absorptivity/emissivity spectra of a synergistic solar and radiative dynamic heat-managing device have exactly the opposite requirement for heating and cooling modes. (b) To switch between solar heating and radiative cooling, the TCE must be transparent to both solar and mid-IR radiation while being highly conductive. (c) Schematic of the proposed UWB-TCE. The monolayer graphene provides uniform local conductance for charge transport, and the gold microgrid is responsible for long-range conductance with only minimal shadow loss of transmittance.

low thermal emissivity works resulting in solar heating (Figure 1a). Note that absorptivity equals emissivity according to Kirchhoff's radiation law. Electrochromic devices (ECDs) are a promising technology for a smart building envelope for net-zero energy buildings. Substantial progress has been made in various aspects, ranging from fundamental materials and photonic science to system-level field testing and commercialization. In particular, metal- and oxide-based ECDs both have show exciting performance and functionality as smart windows in the past decade,[31−39] and polymer-based ECDs are appealing for the variety of color choices and flexibility.[40−42] Other types of smart windows with triggers from temperature, photon, or mechanical strain also have unique advantages and suitable application scenarios.[43−49] Nevertheless, the tunable wavelength range was mainly for the solar spectrum, and the advantage of mid-IR tuning has been overlooked. On the other hand, ECDs specifically designed for mid-IR have been reported,[50−54] but the solar heat gain modulation was not considered. Indeed, the challenge to accomplish wideband and opposite emissivity modulation (Figure 1a) is nontrivial. Most pioneering works, although original and inspiring, showed suboptimal optical property combination, i.e., low thermal emissivity at radiative cooling state or high thermal emissivity at solar heating state.[55,56] A roll-to-roll device was recently reported to be able to effectively switch between solar heating and subambient daytime radiative cooling by mechanically moving the heating/cooling film and creating reversible thermal contact.[57] Nonetheless, the working principle involves moving parts and may need further research for wide employment in buildings.

One major missing piece to realize an electrochromic device that manages both sunlight and thermal radiation is the transparent conducting electrode (TCE). In the last 10 years, great progress has been made in both fundamental research and fabrication technology.[58−62] As shown in Figure 1b, only when the TCE is transparent to both solar and mid-IR

https://doi.org/10.1021/acsenergylett.1c01486
ACS Energy Lett. 2021, 6, 3906−3915

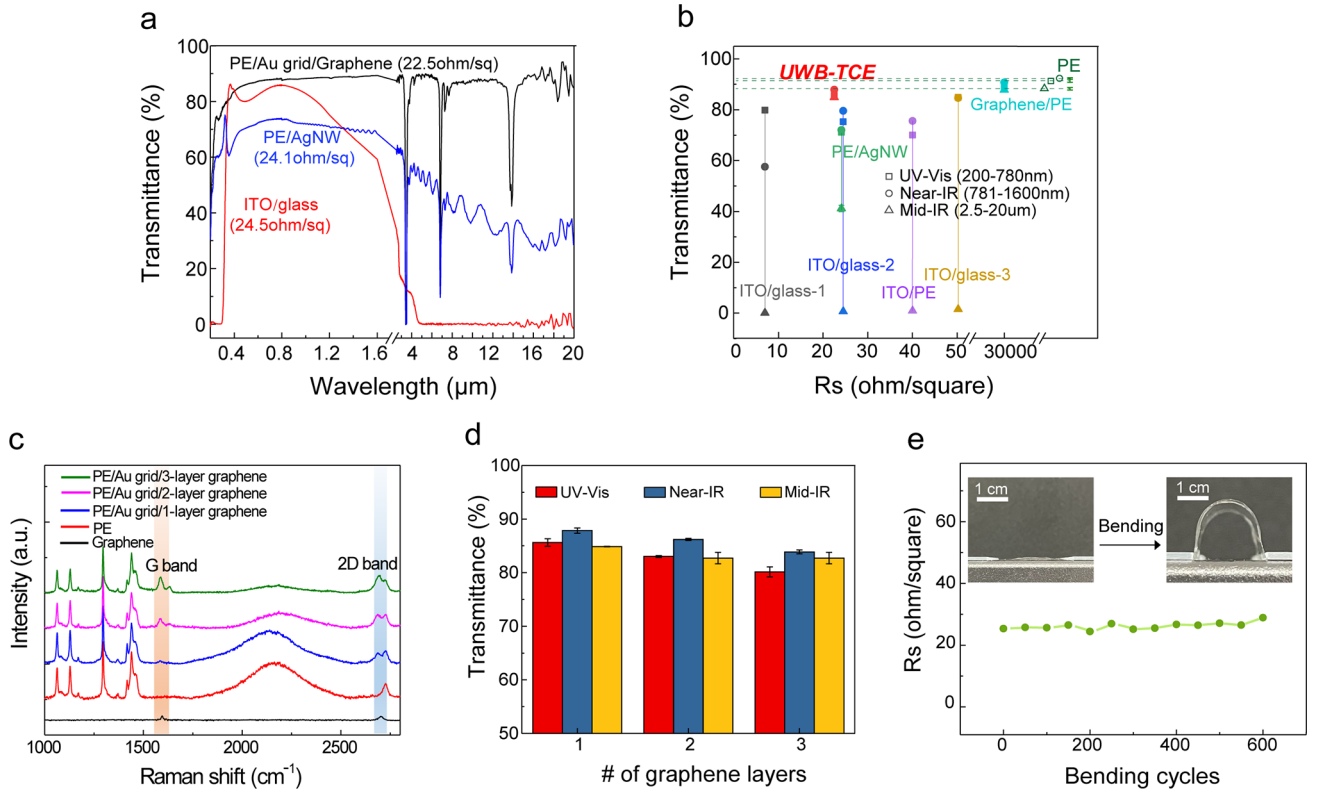

Figure 2. Ultra-wideband transparent conducting electrode (UWB-TCE) and its characteristics. (a) Wideband transmittance spectra of UWTCE and other types of TCE from 0.2 to 20 μm. (b) TCE performance of sheet resistance versus transmittance in UV−vis, NIR, and MIR wavelength regimes. (c) Raman spectra of different layers of graphene on the electrode. (d) UV−vis, NIR, and MIR transmittance of different layers graphene on the electrode. (e) Cyclic bending test with bending radius of 1 cm.

radiation can the underlying electrochromic components be effective; otherwise, the performance will always be limited by the TCE. Take indium tin oxide (ITO) for example: ITO has decent transmittance in the visible and near-IR region that can allow the control of sunlight. However, ITO is opaque and highly reflective in mid-IR and therefore has a low emissivity/absorptivity (Kirchhoff's law). As a result, the overall thermal emissivity will always be low, limiting the cooling performance. Similar argument applies for materials that are opaque and highly absorptive, too. Here, we designed and demonstrated an ultra-wideband transparent conducting electrode (UWB-TCE) with low sheet resistance and high optical transmittance in the wavelength of 0.2−20 μm to allow the underlying active material to fully perform its solar/radiative heat management by varying the electrochemical potential. The UWB-TCE is composed of monolayer graphene, gold microgrid, and polyethylene (PE) membrane (Figure 1c). Monolayer graphene and gold microgrid can provide local and long-range conductance, respectively, which guarantee uniform property change and low ohmic loss. PE film is an IR-transparent flexible substrate. With the UWB-TCE as the working electrode, we demonstrate the plasmonic ECD using Ag−Cu solution as the electrochromic material system. For mid-IR radiative tuning only, the ECD can vary its emissivity (weighted average by 300 K blackbody radiation) between 0.12 and 0.94. This large emissivity contrast of 0.82 is among the highest reported values to date. The ultra-wideband transmittance further allows us to vary between solar heating and radiative cooling via controlling plasmonic absorption. The solar absorptivity (α) and thermal emissivity (ε) of solar heating and radiative cooling mode are (α, ε) = (0.60, 0.20) and (0.33, 0.94), respectively. With the high transmittance in both solar and thermal radiation regimes, our UWB-TCE can be a new key component for an electrically tunable device in multispectral thermal energy management and display and find useful applications in areas such as sustainability, energy, consumer electronics, military and civil applications, and personal health.

Graphene has been regarded as a promising TCE material because of its high carrier mobility and angstrom-level thickness.[63−65] The unique Dirac cone band structure of monolayer graphene results in a constant and wavelength-independent transmittance of $T \approx 1 - \pi\alpha = 1 - \frac{\pi e^2}{\hbar c} = 1 - 2.3\% = 97.7\%$.[66] This broadband multispectral feature makes monolayer graphene the most ideal material for UWB-TCE. The gold microgrid is 10 μm in width with 1 mm spacing; therefore, the shadow loss is only 2%. According to the wire mesh screen model,[67] this small shadow loss can also be regarded as wavelength-independent up to the cutoff wavelength that is on the order of 1 mm in free space or 0.3 THz in the radio frequency domain. Meanwhile, the gold microgrid can significantly reduce the long-range sheet resistance, which is essential for fast and efficient electrochromic switching. The choice of microgrid geometry is apparently the outcome of optimization among electrochemical reaction kinetics, electromagnetic wave transmittance, and materials' intrinsic properties, and we anticipate our proof-of-concept demonstration in solar and mid-IR synergistic heat management contains broader impact for other electromagnetic wavelengths and applications. Finally, PE film is

https://doi.org/10.1021/acsenergylett.1c01486
ACS Energy Lett. 2021, 6, 3906−3915

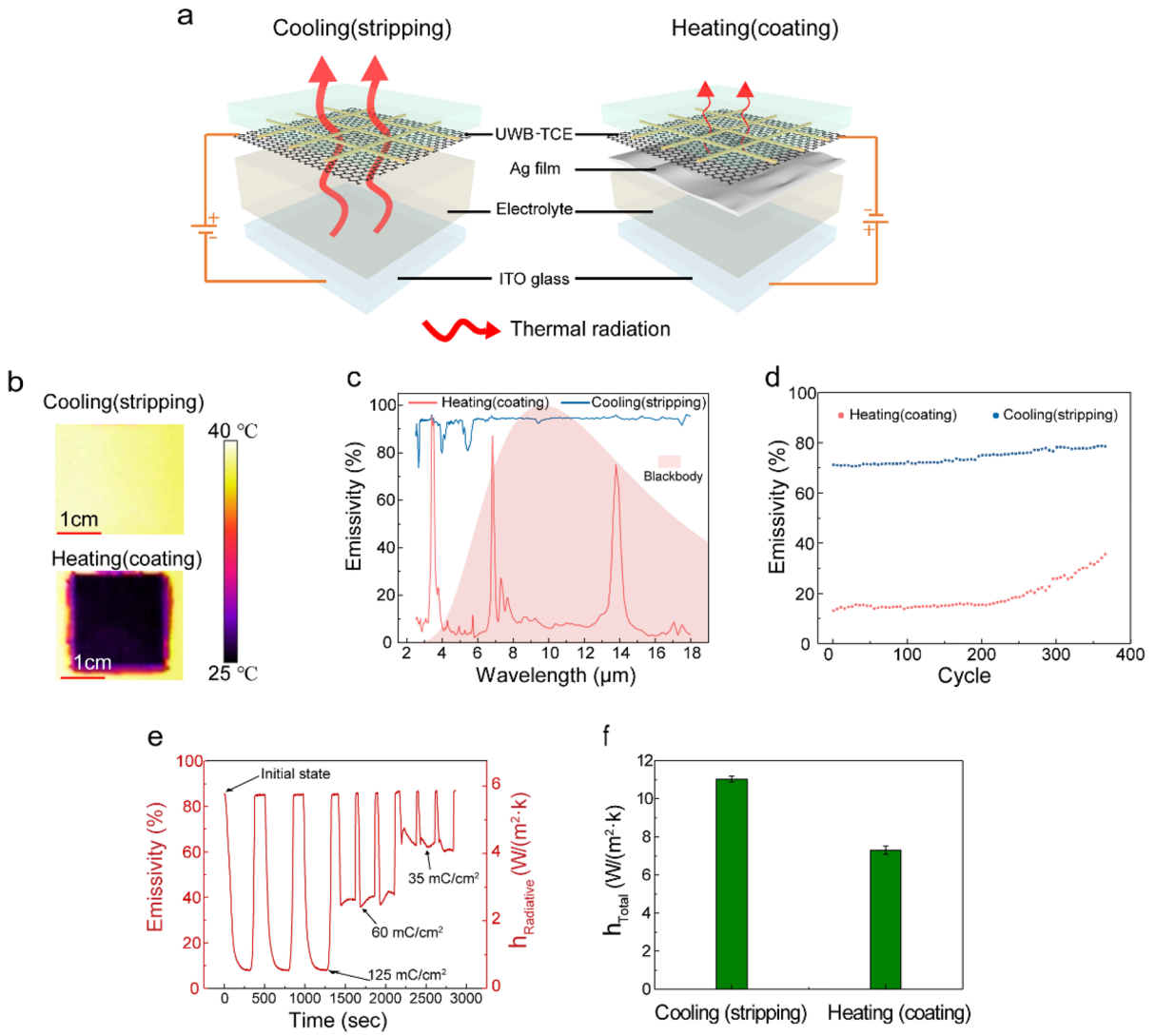

Figure 3. Radiative heat management achieved by UWB-TCE and metal-based electrochromism. (a) Schematic diagram of the IR electrochromic device. Because of the broadband transmittance of UWB-TCE, the emissivity is determined by the underlying electrolyte/metal at the cooling/heating mode. (b) Thermal images and (c) emissivity spectra of the device at cooling and heating modes. (d) Weighted-average emissivity at cooling and heating states versus cycles. The deposition charge density was 125 mC/cm^2 in heating state in (b–d). (e) Controlling the devices at different emissivities (λ = 10 μm). The deposition charge density for emissivity of 0.1, 0.4, and 0.7 were 125, 60, and 35 mC/cm^2, respectively. The calculated radiative heat-transfer coefficients are shown as the secondary y-axis. (f) Total heat-transfer coefficients measured by the guard heater method in an environmental chamber.

chosen as the substrate for its broadband transmittance from visible light to mid-IR. Its mechanical flexibility and low cost are also important features for large-scale adoption, similar to roll-to-roll low-emissivity window films for retrofitting applications.

The broadband transmittance of our UWB-TCE can be clearly shown by comparing with other common TCEs with approximately the same sheet resistance of 22–25 ohm/sq. As shown in Figure 2a, ITO/glass, the most common TCE, exhibits the cutoff below 350 nm of ultraviolet (UV) because of interband absorption.[68] The transmittance is higher in the visible light range but then begins to decline at near-IR because of reflection loss by free carriers. The transmittance is nearly zero at mid-IR. AgNW/PE has a flatter spectrum, but the overall value is much lower in the visible regime at around 70%, which also decreases as the wavelength increases. On the basis of scanning electron microscopy (SEM) images (Figure S1), the decrease is likely caused by the reflection of AgNW mesh with smaller hole sizes.[69] Our UWB-TCE shows the flattest spectrum with slow decay in the deep UV and narrow absorption peaks in mid-IR, both caused by the PE substrate. It is worth noting that this decrease of transmittance, while insignificant, can be further mitigated by removing the impurities and increasing the molecular weight and chain orientation,[70] thereby further boosting the performance of UWB-TCE.

In Figure 2b, we further measured the sheet resistance (R_s) and made the R_s–T plot for various TCEs. The transmittance is represented based on three bands: UV–visible (0.2–0.78 μm), near-IR (0.78–1.6 μm), and mid-IR (2.5–20 μm), which are weight-averaged based on AM1.5 hemispherical solar radiation (ASTM G-173)[71] or 300 K blackbody radiation via Planck's law. All three data points of UWB-TCE are in the upper left area, representing the best overall performance: R_s = 22.4 ohm/sq, T_{UV-vis} = 85.63%, $T_{near-IR}$ = 87.85%, and T_{mid-IR} = 84.87%. If the PE substrate effect is eliminated, the

https://doi.org/10.1021/acsenergylett.1c01486
ACS Energy Lett. 2021, 6, 3906–3915

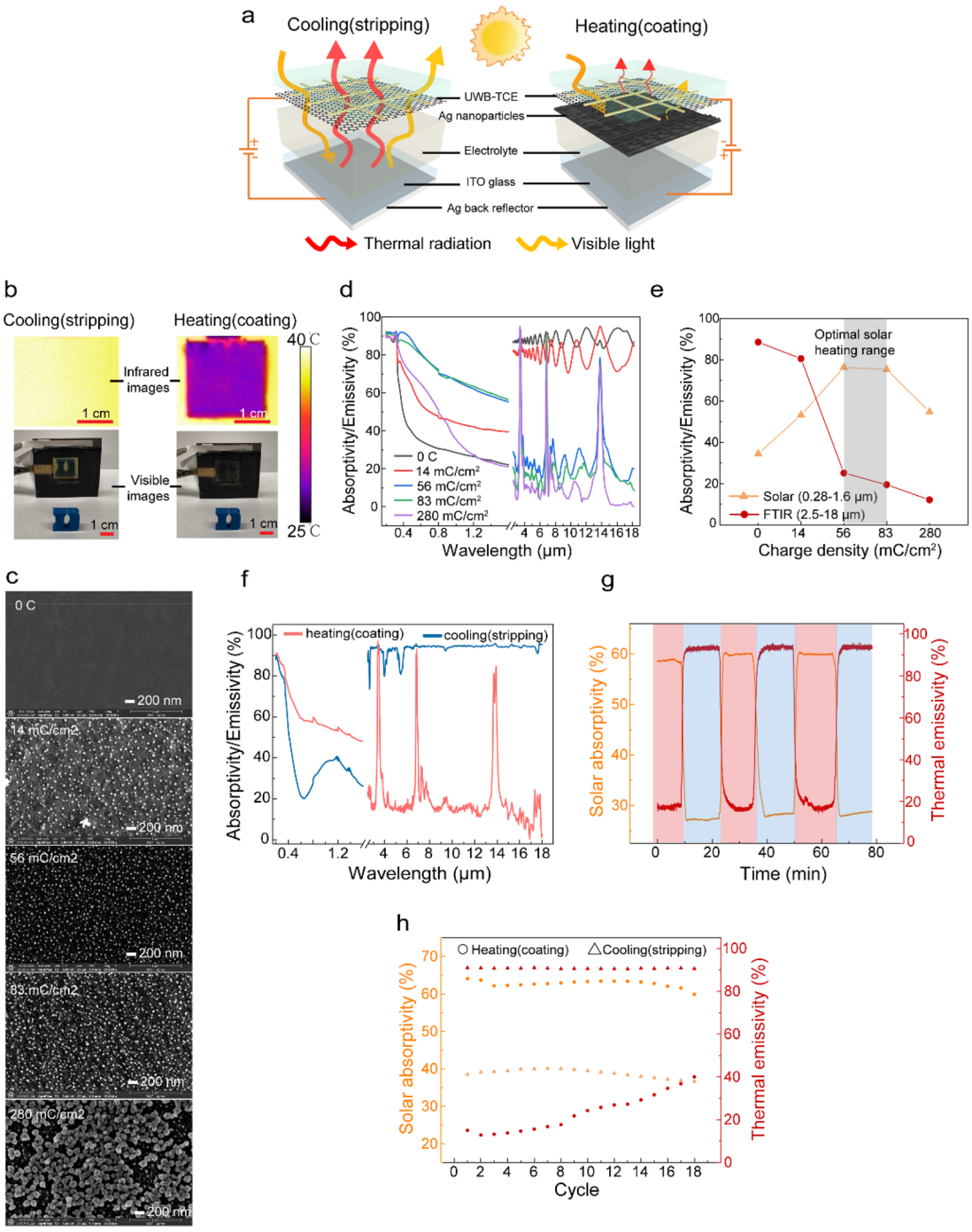

Figure 4. Experimental demonstration of synergistic solar and mid-IR radiative heat management. (a) Schematic of the electrochromic device working principle. The emissivity is determined by the layer beneath the UWB-TCE, and the solar reflectivity is determined by the Ag back reflector at the stripped state and by the Ag nanoparticles at the coated state. (b) The visible (bottom row) and infrared (top row) images of device at cooling and heating states. The cooling mode behaves as a high-emissivity solar reflector, and the heating mode behaves as a low-emissivity solar absorber. (c) SEM images and (d) solar and mid-IR absorptivity/emissivity spectra. (e) weighted-average absorptivity/emissivity of the deposited metals on UWB-TCE film at different charge densities. (f) Spectra of solar absorption and infrared emittance of device at the cooling and heating states. Solar absorptivity (λ = 550 nm) and infrared emissivity (λ = 10 μm) at cooling and heating states by controlling device with several cycles with 0.5 nm thickness of Pt (g) and 0.75 nm thickness of Pt (h). The electrodeposited charge density is 75 mC/cm^2 in the heating state for panels b, f, g, and h.

transmittance will become 94.24%, 95.56%, and 96.62%, respectively.

We further investigated the effect of the number of graphene layers on the electrical sheet resistance and optical properties of UWB-TCE. Figure 2c shows the Raman spectra of UWB-TCE of different layer numbers as well as pure graphene and PE substrate as references. The increased intensity ratio of G to 2D band (I_G/I_{2D}) and the upshift of 2D band position, as shown in Figure S3 and Table S1, which confirm the increase in the number of graphene layer.[72] As the number of layers increases, transmittance decreases stepwise as expected (Figure 2d). Although a greater number of layers decreases the local

https://doi.org/10.1021/acsenergylett.1c01486
ACS Energy Lett. 2021, 6, 3906−3915

resistance, the benefit is outweigh by the optical loss because the gold microgrid is already responsible for most of the electron transport at the device level. In practice, for radiative cooling, suppressing solar absorptivity is essential because of the high intensity of solar radiation; therefore, it is more desirable to choose transmittance over sheet resistance. Moreover, if ohmic loss became critical, reducing the spacing of the gold grid is still the preferred solution because it will increase the device reflectance rather than absorption. Finally, the material choice combination provides UWB-TCE with mechanical flexibility. The sheet resistance remained stable during 600 bending cycles at the radius of 1 cm (Figure 2e).

As demonstrated in the previous comparison with ITO and AgNW (Figure 2a), the mid-IR transmittance of UWB-TCE is indeed a remarkable feature. Therefore, we first demonstrate its utility to regulate infrared radiation by the metal-based electrochromism using UWB-TCE as the working electrode, ITO glass as the counter electrode, and gel electrolyte containing silver and copper ions. A small quantity of copper ions was added to be codeposited with silver, which facilitate reversible deposition through Cu^+ mediation.[37−39] The electrochemical reaction loop is closed by the Br_3^-/Br^- redox couple supplied by tetrabutylammonium bromide (TBABr). We note that a recent study[54] used Ag-based electrochromism for thermal camouflage using percolating semicontinuous Pt film as the electrode.

The initial state of the device (stripped state) is shown in Figure 3a. Because UWB-TCE is transparent in mid-IR, the emissivity is determined by the underlying electrolyte. Most polar solvents, including DMSO and water, are strongly IR-active and absorbing. As the Kirchhoff's radiation law states that spectral absorptivity and spectral emissivity are equal at thermal equilibrium, the stripped state has high emissivity because of the electrolyte and thus works in the radiative cooling mode. Note the choice of the ITO/glass does not influence the emissivity tuning because all the mid-IR emissivity is determined by the IR-absorbing (and thus IR-emitting) electrolyte.

The device can be switched from cooling (high-ε) to heating (low-ε) by electrodepositing metal onto the UBW-TCE. Three-electrode cyclic voltammetry was implemented to investigate the electrochemical potentials of metal deposition and dissolution. As illustrated in (Figure S2), when the potential exceeds 1.5 V during the negative potential sweep, the cathodic current begins to increase sharply, which was attributed to the deposition of Cu and Ag. As a result, silver and copper metals were codeposited gradually to form a thin layer of metals. The low-emissivity metal layer therefore dominates the device radiative property and decreases the thermal radiation significantly, as captured by the thermal camera (Figure 3b and Supporting Information video). This mode is the heating state because of the suppression of radiative heat loss. When a positive voltage (+0.1 V) is applied to the UWB-TCE, the Ag−Cu metals are oxidized to ions and dissolved into the electrolyte, and the device goes back to the initial cooling state. Fourier-transform infrared spectroscopy (FTIR) was used to characterize the emissivity (absorptivity) spectra of the device at two modes. Because the device is IR-opaque, we measured the reflectivity (ρ) and calculate the absorptivity (α) by $\alpha = 1 - \rho$, and Kirchhoff's law is used again to obtain the emissivity, i.e., $\varepsilon = \alpha$. Both heating and cooling modes show broadband emissivity spectra, which is advantageous for thermoregulation. The heating mode spectrum exhibits the same characteristic absorption peaks of PE.

Figure 3d shows the IR-electrochromic device can maintain large emissivity contrast for up to 200 cycles and retained 80% of the value after 350 cycles. We note the low-emissivity state degrades more than the high-emissivity state, which may be due to irreversible formation of metal chlorides or oxides. Furthermore, the electrochromic device can operate in various emissivities, which is a great advantage for providing continuous and high-precision radiative thermoregulation. As shown in Figure 3e, the device's emissivity can be maintained at 0.1, 0.4, and 0.7 by controlling the electrodeposited charge density to 125, 60, and 35 mC/cm^2, respectively. The radiative heat-transfer coefficients can be calculated by

$$h_{\text{radiative}} = 4\sigma\varepsilon T^3$$

where σ is the Stefan−Boltzmann constant, ε the thermal emissivity of device, and T the average of the device surface temperature and the ambient temperature.

To experimentally demonstrate the radiative thermal property, we used the guard heater method in a temperature-controlled chamber to measure the total heat-transfer coefficients which include both radiation and natural convection. The total heat-transfer coefficients of cooling and heating modes were 11.02 and 7.31 W/(m^2·K) respectively. If we assume the temperature difference between the object and the ambience is 10 °C, then the ECD can effectively modulate the heat flux by 37.1 W/m^2. As a rule-of-thumb comparison, this amount of thermoregulation is more than one-third of the human body metabolic heat rate (∼100 W/m^2) or a typical cooling load for a modern house (one ton of air conditioning per 400 sq ft), which indicate its substantial impact on these applications. The advantage can be further emphasized by noting the modulated heat flux is through controlling the "valve" of heat loss rather than directly pumping the thermal power in/out of the object, so the operational power consumption is only for switching states or compensating for non-Faradaic capacity loss, rather than for constantly supplying heat/work.

The metal-based electrochromism not only has exceptional emissivity modulation capability but can also perform solar/mid-IR dual-band synergistic thermoregulation after implementing two modifications: metal morphology optimization and solar reflector (Figure 4a). When the electrodeposited metal is discontinuous with proper particle sizes and distribution, it becomes a plasmonic selective absorber.[73,74] Specifically, random metal nanoparticles and nanoclusters result in broadband localized surface plasmon resonance that is strongly absorbing in the solar spectrum. For mid-IR that has much longer wavelengths, the optical properties are dictated by the effective medium theory, which means the emissivity (absorptivity) is lower by the metallic component. For radiative cooling, a silver mirror is deposited onto the backside of the ITO glass counter electrode and serves as the solar reflector. The mid-IR emissivity is still determined by the electrolyte. The overall effect is a high-emissivity solar reflector, the same as the passive daytime radiative coolers. Essentially, the solar/mid-IR ECD operates between the stripped state and the metal nanoparticle state, and the back reflector rejects the solar heat gain to promote daytime cooling.

As shown in Figure 4b, when the working electrode is stripped (transparent), the underlying silver mirror can reflect visible light and show the blue letter "*D*", meanwhile, thermal

https://doi.org/10.1021/acsenergylett.1c01486
ACS Energy Lett. 2021, 6, 3906−3915

imaging shows the high emissivity. Note the higher nominal IR temperature indicates higher radiosity/emissivity rather than true temperature. As negative bias is applied to the UWB-TCE, electrodeposition begins, and Ag nanoparticles start to nucleate. Before the Ag grows into a thin film as in Figure 4a, there exists an optimal state where the deposit is very close to the percolation threshold, which exhibits both plasmonic absorption of visible light and classical Drude metal reflection of mid-IR radiation.[75,76] As a result, the device appears black and cannot show the blue letter "*D*" anymore, and its thermal image also shows low emissivity (high reflectivity). These visible and IR photos in Figure 4b clearly demonstrate the synergistic solar and mid-IR radiative heat management.

We further study the near-percolation phenomenon by correlating the surface morphology (Figure 4c) with optical measurement results (Figure 4d,e). Indeed, as the deposited Ag increases from 0 to 280 mC/cm^2, the nanoparticles gradually grow and merge into a percolating porous film. On the basis of effective medium approximations (EMA) theory,[77] for long-wavelength light such as mid-IR, the electrodeposited silver can be seen as a whole, so the emissivity decreases monotonically as the more Ag is deposited (Figure 4e, red). On the other hand, the solar absorptivity shows a non-monotonic "volcano" shape, which increases initially from 0.34 (0 mC/cm^2) to 0.76 (56 mC/cm^2) and 0.75 (83 mC/cm^2) and finally decreases to 0.55 (280 mC/cm^2). The outcome is that the device has both high solar absorption and low mid-IR emissivity between 56 and 83 mC/cm^2, which corresponds to the heating mode. Finally, to demonstrate the electrochromic dual-band synergistic heat management, we switched the device between 0 and 75 mC/cm^2 and measured the solar absorption and infrared emissivity spectra and time series (Figure 4f,g). The device exhibits a decent switching speed and contrast of 0.74 in mid-IR and 0.27 in solar bands. Although the solar reflectivity at the cooling mode is not high enough to accomplish subambient cooling, the current performance of the solar-mid-IR dual-band synergistic heat modulation provides a promising design platform for further development in both interfacial electrochemistry and device thermal engineering.

In summary, we successfully demonstrated a graphene-based UWB-TCE with ultra-wideband (0.2−20 μm) high transparency and low sheet resistance, which is the key missing component to accomplish electrochromic devices for both IR tuning and synergistic solar and mid-IR dual-band heat management. The electrochromic device is based on reversible metal deposition, which exhibited high contrast in the mid-IR range (2.5−18 μm) and good cycling performance (>360 cycles) for thermal radiation tuning. The large tunable apparent temperature range of ∼15 °C under 40 °C environment makes it attractive in thermal regulation and energy saving. The synergistic solar/mid-IR dual-band tuning is accomplished by optimizing between near-percolation plasmonic solar absorption and effective medium approximation mid-IR reflection, which dynamically switches between solar heating and radiative cooling with contrast in solar and mid-IR wavelengths of 0.27 and 0.74, respectively. As the first demonstration of UWB-TCE and electrochromic synergistic solar/mid-IR device, the current solar absorptivity is not yet low enough to produce subambient cooling.[15−28] Further improvement of electrolytes and other components' properties or incorporating optical scatterers would be needed to boost the cooling performance. On the other hand, for solar heating, how to delay the percolation threshold so that the metal film can be darker at high mass loading would be a possible direction. Besides solar and mid-IR broadband tuning, individual control of visible color and/or the near-IR property via plasmonic resonance will also be of great practical interest.[33,74]

It should be noted that our UWB-TCE can also apply to other types of electrochromic devices after proper device engineering and surface treatment, which can bring a plethora of future opportunities. The electrochromic device must also have a wholistic consideration for other performance metrics such as switching efficiency, speed, durability, and real heat transport optimization. We anticipate that further development of the graphene UWB-TCE, reversible metal electrodeposition, and photonic structure design can lead to more powerful multispectral and multimodal heat management that can find immense applications for sustainable energy, wearable devices, green buildings, and consumer electronics.

■ ASSOCIATED CONTENT

Supporting Information

The Supporting Information is available free of charge at https://pubs.acs.org/doi/10.1021/acsenergylett.1c01486.

Experimental methods, sample characterization, and Figures S1−S5 (PDF)

Dynamic IR response of the UWB-TCE-based device (MP4)

■ AUTHOR INFORMATION

Corresponding Author

Po-Chun Hsu − *Thomas Lord Department of Mechanical Engineering and Materials Science, Duke University, Durham, North Carolina 27708, United States;* orcid.org/0000-0002-6509-9377; Email: pochun.hsu@duke.edu

Authors

Yunfei Rao − *Thomas Lord Department of Mechanical Engineering and Materials Science, Duke University, Durham, North Carolina 27708, United States; College of Textiles, Donghua University, Shanghai 201620, China*

Jingyuan Dai − *Thomas Lord Department of Mechanical Engineering and Materials Science, Duke University, Durham, North Carolina 27708, United States*

Chenxi Sui − *Thomas Lord Department of Mechanical Engineering and Materials Science, Duke University, Durham, North Carolina 27708, United States*

Yi-Ting Lai − *Thomas Lord Department of Mechanical Engineering and Materials Science, Duke University, Durham, North Carolina 27708, United States*

Zhe Li − *College of Textiles, Donghua University, Shanghai 201620, China*

Haoming Fang − *Thomas Lord Department of Mechanical Engineering and Materials Science, Duke University, Durham, North Carolina 27708, United States*

Xiuqiang Li − *Thomas Lord Department of Mechanical Engineering and Materials Science, Duke University, Durham, North Carolina 27708, United States*

Wei Li − *College of Textiles, Donghua University, Shanghai 201620, China*

Complete contact information is available at: https://pubs.acs.org/10.1021/acsenergylett.1c01486

Author Contributions

†Y.R., J.D., C.S., and Y.-T.L. contributed equally to this work.

Notes

The authors declare no competing financial interest.

■ ACKNOWLEDGMENTS

The authors thank the Pratt School of Engineering at Duke University for the funding support and the Shared Materials Instrumentation Facility (SMIF) for its technical support. Y.R. also acknowledges the China Scholarship Council for their financial support.

■ REFERENCES

(1) International Energy Agency. *World energy balances: database documentation* (2020 edition); https://www.iea.org/data-and-statistics/data-product/world-energy-statistics-and-balances (accessed 2021-10-08).

(2) Department of Energy. *Heating & Cooling*; http://www.energy.gov/heating-cooling (accessed 2021-10-08).

(3) Li, X.; Xie, W.; Sui, C.; Hsu, P.-C. Multispectral Thermal Management Designs for Net-Zero Energy Buildings. *ACS Materials Letters* **2020**, *2* (12), 1624−1643.

(4) Kraemer, D.; Poudel, B.; Feng, H.-P.; Caylor, J. C.; Yu, B.; Yan, X.; Ma, Y.; Wang, X.; Wang, D.; Muto, A.; McEnaney, K.; Chiesa, M.; Ren, Z.; Chen, G. High-performance flat-panel solar thermoelectric generators with high thermal concentration. *Nat. Mater.* **2011**, *10* (7), 532−538.

(5) Cao, F.; McEnaney, K.; Chen, G.; Ren, Z. A review of cermet-based spectrally selective solar absorbers. *Energy Environ. Sci.* **2014**, *7* (5), 1615−1627.

(6) Ghasemi, H.; Ni, G.; Marconnet, A. M.; Loomis, J.; Yerci, S.; Miljkovic, N.; Chen, G. Solar steam generation by heat localization. *Nat. Commun.* **2014**, *5*, 4449.

(7) Boriskina, S.; Green, M. A.; Catchpole, K.; Yablonovitch, E.; Beard, M. C.; Okada, Y.; Lany, S.; Gershon, T.; Zakutayev, A.; Tahersima, M.; Sorger, V. J.; Naughton, M. J.; Kempa, K.; Dagenais, M.; Yao, Y.; Xu, L.; Sheng, X.; Bronstein, N. D.; Rogers, J. A.; Alivisatos, A. P.; Nuzzo, R. G.; Gordon, J. M.; Wu, D. M.; Wisser, M. D.; Salleo, A.; Dionne, J.; Bermel, P.; Greffet, J. J.; Celanovic, I.; Soljacic, M.; Manor, A.; Rotschild, C.; Raman, A.; Zhu, L.; Fan, S.; Chen, G. Roadmap on optical energy conversion. *J. Opt.* **2016**, *18* (7), 073004.

(8) Zhou, Z.; Sakr, E.; Sun, Y.; Bermel, P. Solar thermophotovoltaics: reshaping the solar spectrum. *Nanophotonics* **2016**, *5* (1), 1−21.

(9) Mandal, J.; Wang, D.; Overvig, A. C.; Shi, N. N.; Paley, D.; Zangiabadi, A.; Cheng, Q.; Barmak, K.; Yu, N.; Yang, Y. Scalable, "Dip-and-Dry" Fabrication of a Wide-Angle Plasmonic Selective Absorber for High-Efficiency Solar−Thermal Energy Conversion. *Adv. Mater.* **2017**, *29* (41), 1702156.

(10) Tao, P.; Ni, G.; Song, C.; Shang, W.; Wu, J.; Zhu, J.; Chen, G.; Deng, T. Solar-driven interfacial evaporation. *Nature Energy* **2018**, *3*, 1031−1041.

(11) Chen, M.; Mandal, J.; Ye, Q.; Li, A.; Cheng, Q.; Gong, T.; Jin, T.; He, Y.; Yu, N.; Yang, Y. A Scalable Dealloying Technique To Create Thermally Stable Plasmonic Nickel Selective Solar Absorbers. *ACS Applied Energy Materials* **2019**, *2* (9), 6551−6557.

(12) Granqvist, C. G.; Hjortsberg, A. Radiative cooling to low temperatures: General considerations and application to selectively emitting SiO films. *J. Appl. Phys.* **1981**, *52*, 4205.

(13) Eriksson, T. S.; Granqvist, C. G. Radiative cooling computed for model atmospheres. *Appl. Opt.* **1982**, *21* (23), 4381−4388.

(14) Zhu, X. Radiative Cooling Calculated by Random Band Models with S-1-β Tailed Distribution. *J. Atmos. Sci.* **1989**, *46* (4), 511−520.

(15) Raman, A. P.; Anoma, M. A.; Zhu, L.; Rephaeli, E.; Fan, S. Passive radiative cooling below ambient air temperature under direct sunlight. *Nature* **2014**, *515*, 540−544.

(16) Shi, N. N.; Tsai, C.-C.; Camino, F.; Bernard, G. D.; Yu, N.; Wehner, R. Keeping cool: Enhanced optical reflection and radiative heat dissipation in Saharan silver ants. *Science* **2015**, *349* (6245), 298−301.

(17) Hsu, P.-C.; Song, A. Y.; Catrysse, P. B.; Liu, C.; Peng, Y.; Xie, J.; Fan, S.; Cui, Y. Radiative human body cooling by nanoporous polyethylene textile. *Science* **2016**, *353* (6303), 1019−1023.

(18) Zhai, Y.; Ma, Y.; David, S. N.; Zhao, D.; Lou, R.; Tan, G.; Yang, R.; Yin, X. Scalable-manufactured randomized glass-polymer hybrid metamaterial for daytime radiative cooling. *Science* **2017**, *355* (6329), 1062−1066.

(19) Bhatia, B.; Leroy, A.; Shen, Y.; Zhao, L.; Gianello, M.; Li, D.; Gu, T.; Hu, J.; Soljačić, M.; Wang, E. N. Passive directional sub-ambient daytime radiative cooling. *Nat. Commun.* **2018**, *9*, 5001.

(20) Li, W.; Shi, Y.; Chen, Z.; Fan, S. Photonic thermal management of coloured objects. *Nat. Commun.* **2018**, *9*, 4240.

(21) Mandal, J.; Fu, Y.; Overvig, A. C.; Jia, M.; Sun, K.; Shi, N. N.; Zhou, H.; Xiao, X.; Yu, N.; Yang, Y. Hierarchically porous polymer coatings for highly efficient passive daytime radiative cooling. *Science* **2018**, *362* (6412), 315−319.

(22) Shi, N. N.; Tsai, C.-C.; Carter, M. J.; Mandal, J.; Overvig, A. C.; Sfeir, M. Y.; Lu, M.; Craig, C. L.; Bernard, G. D.; Yang, Y.; Yu, N. Nanostructured fibers as a versatile photonic platform: radiative cooling and waveguiding through transverse Anderson localization. *Light: Sci. Appl.* **2018**, *7*, 37.

(23) Leroy, A.; Bhatia, B.; Kelsall, C. C.; Castillejo-Cuberos, A.; Di Capua, H. M.; Zhao, L.; Zhang, L.; Guzman, A. M.; Wang, E. N. High-performance subambient radiative cooling enabled by optically selective and thermally insulating polyethylene aerogel. *Science Advances* **2019**, *5* (10), No. eaat9480.

(24) Li, T.; Zhai, Y.; He, S.; Gan, W.; Wei, Z.; Heidarinejad, M.; Dalgo, D.; Mi, R.; Zhao, X.; Song, J.; Dai, J.; Chen, C.; Aili, A.; Vellore, A.; Martini, A.; Yang, R.; Srebric, J.; Yin, X.; Hu, L. A radiative cooling structural material. *Science* **2019**, *364* (6442), 760−763.

(25) Zhao, D.; Aili, A.; Yin, X.; Tan, G.; Yang, R. Roof-integrated radiative air-cooling system to achieve cooler attic for building energy saving. *Energy and Buildings* **2019**, *203*, 109453.

(26) Zhao, D.; Aili, A.; Zhai, Y.; Lu, J.; Kidd, D.; Tan, G.; Yin, X.; Yang, R. Subambient Cooling of Water: Toward Real-World Applications of Daytime Radiative Cooling. *Joule* **2019**, *3* (1), 111−123.

(27) Zhou, L.; Song, H.; Liang, J.; Singer, M.; Zhou, M.; Stegenburgs, E.; Zhang, N.; Xu, C.; Ng, T.; Yu, Z.; Ooi, B.; Gan, Q. A polydimethylsiloxane-coated metal structure for all-day radiative cooling. *Nature Sustainability* **2019**, *2*, 718−724.

(28) Zeng, S.; Pian, S.; Su, M.; Wang, Z.; Wu, M.; Liu, X.; Chen, M.; Xiang, Y.; Wu, J.; Zhang, M.; Cen, Q.; Tang, Y.; Zhou, X.; Huang, Z.; Wang, R.; Tunuhe, A.; Sun, X.; Xia, Z.; Tian, M.; Chen, M.; Ma, X.; Yang, L.; Zhou, J.; Zhou, H.; Yang, Q.; Li, X.; Ma, Y.; Tao, G. Hierarchical-morphology metafabric for scalable passive daytime radiative cooling. *Science* **2021**, *373* (6555), 692.

(29) Sartori, I.; Napolitano, A.; Voss, K. Net zero energy buildings: A consistent definition framework. *Energy and Buildings* **2012**, *48*, 220−232.

(30) Wu, W.; Skye, H. M. Residential net-zero energy buildings: Review and perspective. *Renewable Sustainable Energy Rev.* **2021**, *142*, 110859.

(31) Llordés, A.; Garcia, G.; Gazquez, J.; Milliron, D. J. Tunable near-infrared and visible-light transmittance in nanocrystal-in-glass composites. *Nature* **2013**, *500*, 323−326.

(32) Yan, C.; Kang, W.; Wang, J.; Cui, M.; Wang, X.; Foo, C. Y.; Chee, K. J.; Lee, P. S. Stretchable and Wearable Electrochromic Devices. *ACS Nano* **2014**, *8* (1), 316−322.

(33) Eh, A. L.-S.; Lin, M.-F.; Cui, M.; Cai, G.; Lee, P. S. A copper-based reversible electrochemical mirror device with switchability between transparent, blue, and mirror states. *J. Mater. Chem. C* **2017**, *5* (26), 6547−6554.

(34) Cai, G.; Park, S.; Cheng, X.; Eh, A. L.-S.; Lee, P. S. Inkjet-printed metal oxide nanoparticles on elastomer for strain-adaptive transmissive electrochromic energy storage systems. *Sci. Technol. Adv. Mater.* **2018**, *19* (1), 759−770.
(35) Hernandez, T. S.; Alshurafa, M.; Strand, M. T.; Yeang, A. L.; Danner, M. G.; Barile, C. J.; McGehee, M. D. Electrolyte for Improved Durability of Dynamic Windows Based on Reversible Metal Electrodeposition. *Joule* **2020**, *4* (7), 1501−1513.
(36) Strand, M. T.; Hernandez, T. S.; Danner, M. G.; Yeang, A. L.; Jarvey, N.; Barile, C. J.; McGehee, M. D. Polymer inhibitors enable > 900 cm2 dynamic windows based on reversible metal electrodeposition with high solar modulation. *Nature Energy* **2021**, *6*, 546−554.
(37) Araki, S.; Nakamura, K.; Kobayashi, K.; Tsuboi, A.; Kobayashi, N. Electrochemical Optical-Modulation Device with Reversible Transformation Between Transparent, Mirror, and Black. *Adv. Mater.* **2012**, *24* (23), OP122−OP126.
(38) Barile, C. J.; Slotcavage, D. J.; Hou, J.; Strand, M. T.; Hernandez, T. S.; McGehee, M. D. Dynamic Windows with Neutral Color, High Contrast, and Excellent Durability Using Reversible Metal Electrodeposition. *Joule* **2017**, *1* (1), 133−145.
(39) Hernandez, T. S.; Barile, C. J.; Strand, M. T.; Dayrit, T. E.; Slotcavage, D. J.; McGehee, M. D. Bistable Black Electrochromic Windows Based on the Reversible Metal Electrodeposition of Bi and Cu. *ACS Energy Letters* **2018**, *3* (1), 104−111.
(40) Beaujuge, P. M.; Reynolds, J. R. Color Control in π-Conjugated Organic Polymers for Use in Electrochromic Devices. *Chem. Rev.* **2010**, *110* (1), 268−320.
(41) Mortimer, R. J. Electrochromic Materials. *Annu. Rev. Mater. Res.* **2011**, *41*, 241−268.
(42) Cai, G.; Chen, J.; Xiong, J.; Lee-Sie Eh, A.; Wang, J.; Higuchi, M.; Lee, P. S. Molecular level assembly for high-performance flexible electrochromic energy-storage devices. *ACS Energy Letters* **2020**, *5* (4), 1159−1166.
(43) Zhou, Y.; Cai, Y.; Hu, X.; Long, Y. Temperature-responsive hydrogel with ultra-large solar modulation and high luminous transmission for "smart window" applications. *J. Mater. Chem. A* **2014**, *2* (33), 13550−13555.
(44) Zhang, Q.; Wommer, J.; O'Rourke, C.; Teitelman, J.; Tang, Y.; Robison, J.; Lin, G.; Yin, J. Origami and kirigami inspired self-folding for programming three-dimensional shape shifting of polymer sheets with light. *Extreme Mechanics Letters* **2017**, *11*, 111−120.
(45) Ke, Y.; Chen, J.; Lin, G.; Wang, S.; Zhou, Y.; Yin, J.; Lee, P. S.; Long, Y. Smart Windows: Electro-, Thermo-, Mechano-, Photochromics, and Beyond. *Adv. Energy Mater.* **2019**, *9* (39), 1902066.
(46) Ke, Y.; Yin, Y.; Zhang, Q.; Tan, Y.; Hu, P.; Wang, S.; Tang, Y.; Zhou, Y.; Wen, X.; Wu, S.; White, T. J.; Yin, J.; Peng, J.; Xiong, Q.; Zhao, D.; Long, Y. Adaptive Thermochromic Windows from Active Plasmonic Elastomers. *Joule* **2019**, *3* (3), 858−871.
(47) Ke, Y.; Zhang, Q.; Wang, T.; Wang, S.; Li, N.; Lin, G.; Liu, X.; Dai, Z.; Yan, J.; Yin, J.; Magdassi, S.; Zhao, D.; Long, Y. Cephalopod-inspired versatile design based on plasmonic VO2 nanoparticle for energy-efficient mechano-thermochromic windows. *Nano Energy* **2020**, *73*, 104785.
(48) Zhou, C.; Li, D.; Tan, Y.; Ke, Y.; Wang, S.; Zhou, Y.; Liu, G.; Wu, S.; Peng, J.; Li, A.; Li, S.; Chan, S. H.; Magdassi, S.; Long, Y. 3D Printed Smart Windows for Adaptive Solar Modulations. *Adv. Opt. Mater.* **2020**, *8* (11), 2000013.
(49) Zhou, Y.; Wang, S.; Peng, J.; Tan, Y.; Li, C.; Boey, F. Y. C.; Long, Y. Liquid Thermo-Responsive Smart Window Derived from Hydrogel. *Joule* **2020**, *4* (11), 2458−2474.
(50) Chandrasekhar, P.; Zay, B. J.; Lawrence, D.; Caldwell, E.; Sheth, R.; Stephan, R.; Cornwell, J. Variable-emittance infrared electrochromic skins combining unique conducting polymers, ionic liquid electrolytes, microporous polymer membranes, and semiconductor/polymer coatings, for spacecraft thermal control. *J. Appl. Polym. Sci.* **2014**, *131* (19), 40850.
(51) Salihoglu, O.; Uzlu, H. B.; Yakar, O.; Aas, S.; Balci, O.; Kakenov, N.; Balci, S.; Olcum, S.; Süzer, S.; Kocabas, C. Graphene-Based Adaptive Thermal Camouflage. *Nano Lett.* **2018**, *18* (7), 4541−4548.
(52) Zhao, L.; Zhang, R.; Deng, C.; Peng, Y.; Jiang, T. Tunable Infrared Emissivity in Multilayer Graphene by Ionic Liquid Intercalation. *Nanomaterials* **2019**, *9* (8), 1096.
(53) Li, M.; Liu, D.; Cheng, H.; Peng, L.; Zu, M. Graphene-based reversible metal electrodeposition for dynamic infrared modulation. *J. Mater. Chem. C* **2020**, *8* (25), 8538−8545.
(54) Li, M.; Liu, D.; Cheng, H.; Peng, L.; Zu, M. Manipulating metals for adaptive thermal camouflage. *Science Advances* **2020**, *6* (22), No. eaba3494.
(55) Mandal, J.; Du, S.; Dontigny, M.; Zaghib, K.; Yu, N.; Yang, Y. Li4Ti5O12: A Visible-to-Infrared Broadband Electrochromic Material for Optical and Thermal Management. *Adv. Funct. Mater.* **2018**, *28* (36), 1802180.
(56) Ergoktas, M. S.; Bakan, G.; Kovalska, E.; Le Fevre, L. W.; Fields, R. P.; Steiner, P.; Yu, X.; Salihoglu, O.; Balci, S.; Fal'ko, V. I.; Novoselov, K. S.; Dryfe, R. A. W.; Kocabas, C. Multispectral graphene-based electro-optical surfaces with reversible tunability from visible to microwave wavelengths. *Nat. Photonics* **2021**, *15*, 493−498.
(57) Li, X.; Sun, B.; Sui, C.; Nandi, A.; Fang, H.; Peng, Y.; Tan, G.; Hsu, P.-C. Integration of daytime radiative cooling and solar heating for year-round energy saving in buildings. *Nat. Commun.* **2020**, *11*, 6101.
(58) Seo, S.; Min, M.; Lee, S. M.; Lee, H. Photo-switchable molecular monolayer anchored between highly transparent and flexible graphene electrodes. *Nat. Commun.* **2013**, *4*, 1920.
(59) Wu, H.; Kong, D.; Ruan, Z.; Hsu, P.-C.; Wang, S.; Yu, Z.; Carney, T. J.; Hu, L.; Fan, S.; Cui, Y. A transparent electrode based on a metal nanotrough network. *Nat. Nanotechnol.* **2013**, *8*, 421−425.
(60) Liu, N.; Chortos, A.; Lei, T.; Jin, L.; Kim, T. R.; Bae, W.-G.; Zhu, C.; Wang, S.; Pfattner, R.; Chen, X.; Sinclair, R.; Bao, Z. Ultratransparent and stretchable graphene electrodes. *Science Advances* **2017**, *3* (22), No. e1700159.
(61) Lin, S.; Liu, J.; Li, W.; Wang, D.; Huang, Y.; Jia, C.; Li, Z.; Murtaza, M.; Wang, H.; Song, J.; Liu, Z.; Huang, K.; Zu, D.; Lei, M.; Hong, B.; Wu, H. A Flexible, Robust, and Gel-Free Electroencephalogram Electrode for Noninvasive Brain-Computer Interfaces. *Nano Lett.* **2019**, *19* (10), 6853−6861.
(62) Lin, S.; Wang, H.; Wu, F.; Wang, Q.; Bai, X.; Zu, D.; Song, J.; Wang, D.; Liu, Z.; Li, Z.; Tao, N.; Huang, K.; Lei, M.; Li, B.; Wu, H. Room-temperature production of silver-nanofiber film for large-area, transparent and flexible surface electromagnetic interference shielding. *npj Flexible Electronics* **2019**, *3*, 6.
(63) Kim, K. S.; Zhao, Y.; Jang, H.; Lee, S. Y.; Kim, J. M.; Kim, K. S.; Ahn, J.-H.; Kim, P.; Choi, J.-Y.; Hong, B. H. Large-scale pattern growth of graphene films for stretchable transparent electrodes. *Nature* **2009**, *457*, 706−710.
(64) Bae, S.; Kim, H.; Lee, Y.; Xu, X.; Park, J.-S.; Zheng, Y.; Balakrishnan, J.; Lei, T.; Ri Kim, H.; Song, Y. I.; Kim, Y.-J.; Kim, K. S.; Özyilmaz, B.; Ahn, J.-H.; Hong, B. H.; Iijima, S. Roll-to-roll production of 30-in. graphene films for transparent electrodes. *Nat. Nanotechnol.* **2010**, *5*, 574−578.
(65) Wu, J.; Agrawal, M.; Becerril, H. A.; Bao, Z.; Liu, Z.; Chen, Y.; Peumans, P. Organic Light-Emitting Diodes on Solution-Processed Graphene Transparent Electrodes. *ACS Nano* **2010**, *4* (1), 43−48.
(66) Nair, R. R.; Blake, P.; Grigorenko, A. N.; Novoselov, K. S.; Booth, T. J.; Stauber, T.; Peres, N. M. R.; Geim, A. K. Fine Structure Constant Defines Visual Transparency of Graphene. *Science* **2008**, *320* (5881), 1308.
(67) Casey, K. F. Electromagnetic shielding behavior of wire-mesh screens. *IEEE Trans. Electromagn. Compat.* **1988**, *30* (3), 298−306.
(68) Ginley, D. S.; Perkins, J. D. Transparent Conductors. In *Handbook of Transparent Conductors*, Ginley, D. S., Ed.; Springer US: Boston, MA, 2011; pp 1−25.
(69) Hsu, P.-C.; Liu, X.; Liu, C.; Xie, X.; Lee, H. R.; Welch, A. J.; Zhao, T.; Cui, Y. Personal Thermal Management by Metallic Nanowire-Coated Textile. *Nano Lett.* **2015**, *15* (1), 365−371.

https://doi.org/10.1021/acsenergylett.1c01486
ACS Energy Lett. 2021, 6, 3906−3915

(70) Lozano, L. M.; Hong, S.; Huang, Y.; Zandavi, H.; El Aoud, Y. A.; Tsurimaki, Y.; Zhou, J.; Xu, Y.; Osgood, R. M.; Chen, G.; Boriskina, S. V. Optical engineering of polymer materials and composites for simultaneous color and thermal management. *Opt. Mater. Express* **2019**, *9* (5), 1990−2005.
(71) Santiago-Prowald, J.; Baier, H. Advances in deployable structures and surfaces for large apertures in space. *CEAS Space Journal* **2013**, *5*, 89−115.
(72) Ferrari, A. C.; Meyer, J. C.; Scardaci, V.; Casiraghi, C.; Lazzeri, M.; Mauri, F.; Piscanec, S.; Jiang, D.; Novoselov, K. S.; Roth, S.; Geim, A. K. Raman Spectrum of Graphene and Graphene Layers. *Phys. Rev. Lett.* **2006**, *97* (18), 187401.
(73) Tsuboi, A.; Nakamura, K.; Kobayashi, N. A Localized Surface Plasmon Resonance-Based Multicolor Electrochromic Device with Electrochemically Size-Controlled Silver Nanoparticles. *Adv. Mater.* **2013**, *25* (23), 3197−3201.
(74) Wang, G.; Chen, X.; Liu, S.; Wong, C.; Chu, S. Mechanical Chameleon through Dynamic Real-Time Plasmonic Tuning. *ACS Nano* **2016**, *10* (2), 1788−1794.
(75) Smith, G. B.; Maaroof, A. I.; Cortie, M. B. Percolation in nanoporous gold and the principle of universality for two-dimensional to hyperdimensional networks. *Phys. Rev. B: Condens. Matter Mater. Phys.* **2008**, *78* (16), 165418.
(76) Earp, A. A.; Smith, G. B. Evolution of plasmonic response in growing silver thin films with pre-percolation non-local conduction and emittance drop. *J. Phys. D: Appl. Phys.* **2011**, *44*, 255102.
(77) Choy, T. C. *Effective medium theory: principles and applications*. Oxford University Press: 2015; Vol. *165*.

https://doi.org/10.1021/acsenergylett.1c01486
ACS Energy Lett. 2021, 6, 3906−3915